Available online at www.sciencedirect.com
SCIENCE DIRECT®
Toxicology in Vitro 20 (2006) 82–95
Toxicology in Vitro
www.elsevier.com/locate/toxinvit

Differences in dissolution behavior in a phagolysosomal simulant fluid for single-constituent and multi-constituent materials associated with beryllium sensitization and chronic beryllium disease

Aleksandr B. Stefaniak [a,b,*], Gregory A. Day [c,1], Mark D. Hoover [c,2], Patrick N. Breysse [b], Ronald C. Scripsick [a]

[a] *Industrial Hygiene and Safety Group, MS K553, Los Alamos National Laboratory, Los Alamos, NM 87545, United States*
[b] *Division of Environmental Health Engineering, Johns Hopkins University Bloomberg School of Public Health, Baltimore, MD 21205, United States*
[c] *National Institute for Occupational Safety and Health, Centers for Disease Control and Prevention, Mailstop H-2800, Morgantown, WV 26505, United States*

Received 19 April 2005; accepted 15 June 2005
Available online 2 August 2005

Abstract

Particle dissolution within macrophage phagolysosomes is hypothesized to be an important source of dissolved beryllium for input to the cell-mediated immune reaction associated with development of beryllium sensitization and chronic beryllium disease (CBD). To better understand the dissolution of beryllium materials associated with elevated prevalence of sensitization and CBD, single-constituent (beryllium oxide (BeO) particles sampled from a screener operation, finished product BeO powder, finish product beryllium metal powder) and multi-constituent (particles sampled from an arc furnace during processing of copper–beryllium alloy) aerosol materials were studied. Dissolution rates were measured using phagolysosomal simulant fluid (PSF) in a static dissolution technique and then normalized to measured values of specific surface area to calculate a chemical dissolution rate constant (k) for each material. Values of k, in g/(cm^2 day), for screener BeO particles ($1.3 \pm 1.9 \times 10^{-8}$) and for BeO powder ($1.1 \pm 0.5 \times 10^{-8}$) were similar ($p = 0.45$). The value of k observed for beryllium metal powder ($1.1 \pm 1.4 \times 10^{-7}$) was significantly greater than observed for the BeO materials ($p < 0.0003$). For arc furnace particles, k ($1.6 \pm 0.6 \times 10^{-7}$) was significantly greater than observed for the BeO materials ($p < 0.00001$), despite the fact that the chemical form of beryllium in the aerosol was BeO. These results suggest that dissolution of beryllium differs among physicochemical forms of beryllium and direct measurement of dissolution is needed for multi-constituent aerosol. Additional studies of the dissolution behavior of beryllium materials in a variety

Abbreviations: ABDC, alkylbenzyldimethylammonium chloride; ANOVA, one-way analysis of variance; BeO, beryllium oxide; CBD, chronic beryllium disease; CMD, count median diameter; CuO, copper(II) oxide; Cu_2O, copper(I) oxide; ICP-MS, inductively coupled plasma-mass spectroscopy; k, chemical dissolution rate constant; D_m, mass median diameter; $\frac{M}{M_0}$, mass fraction remaining from a log-normally distributed population of homogeneous particles; HCl, hydrochloric acid; M_D, dissolved beryllium mass; M_0, initial particulate beryllium mass; PSF, phagolysosomal simulant fluid; σ_g, geometric standard deviation; σ, $\ln(\sigma_g)$; SUF, serum ultrafiltrate; SSA, specific surface area; SSA_{eff}, effective SSA; US EPA, United States Environmental Protection Agency; XPS, X-ray photoelectron spectroscopy.

* Corresponding author. Current address: National Institute for Occupational Safety and Health, Centers for Disease Control and Prevention, Mailstop H-2800, Morgantown, WV 26505, United States. Tel.: +1 304 285 6302; fax: +1 304 285 6321.
E-mail address: astefaniak@cdc.gov (A.B. Stefaniak).
[1] Former address: Materials Technology and Metallurgy Group, MS K553, Los Alamos National Laboratory, Los Alamos, NM 87545, United States.
[2] Former address: Lovelace Respiratory Research Institute, Albuquerque, NM 87185, United States.

0887-2333/$ - see front matter
doi:10.1016/j.tiv.2005.06.031

of mixture configurations will aid in developing exposure–response models to improve understanding of the risk of beryllium sensitization and CBD.

Keywords: Beryllium; Multi-constituent aerosol; Dissolution; Phagolysosome

1. Introduction

Chronic beryllium disease (CBD) is a progressive lung disease characterized by non-caseating granulomas, interstitial infiltrates, and fibrosis, that occurs in individuals who are sensitized to beryllium (Maier and Newman, 1998). Development of CBD is associated with inhalation of relatively insoluble beryllium metal and oxide particles (Eisenbud, 1998; Kreiss et al., 1997; Sterner and Eisenbud, 1951). Copper–beryllium is also of special concern because elevated prevalence of sensitization and disease have been observed in workers exposed at airborne concentrations of beryllium below the current statutory limit of 2 μg/m^3 (Schuler et al., 2005). At the cellular level, dissolution of particles (conversion from a particle to dissolved beryllium) within phagolysosomes is hypothesized to be an important input to the cell-mediated CBD immune reaction (Eidson et al., 1991; Richeldi et al., 1993). Few studies have evaluated dissolution of beryllium aerosol materials. Finch et al. (1988) evaluated the dissolution of beryllium metal powder and laboratory prepared beryllium oxide (BeO) particles at pH 1 and pH 7.3. No studies have evaluated dissolution of beryllium materials at the pH within phagolysosomes, pH 4.5 (see for example, Nyberg et al., 1989a,b). In the current work, phagolysosomal simulant fluid at pH 4.5 was used to measure dissolution rates for single-constituent and multi-constituent beryllium aerosol materials associated with elevated prevalence of beryllium sensitization and CBD (Kreiss et al., 1997; Stange et al., 1996). Single-constituent aerosols were defined as single chemical compound particles, whereas, multi-constituent aerosols were defined as consisting of a mixture of single-constituent particles, multi-constituent particles, or a mixture of single-constituent particles and multi-constituent particles. We compare the experimental results to published literature, describe how the observed dissolution properties may relate to development of beryllium sensitization and CBD, and discuss how this information can be used to improve worker protection.

2. Materials and methods

2.1. Study overview

We measured dissolution rates for single-constituent and multi-constituent beryllium aerosol materials and modeled results using a surface-area-proportional dissolution model. As noted below, the rate of beryllium dissolution from the multi-constituent aerosol material was greater than expected compared to dissolution of the single-constituent materials. This finding prompted a follow-on experiment in which additional details about the bulk and surface composition of the study materials were used to account for observed beryllium dissolution from the multi-constituent material.

2.2. Beryllium study materials

Finished product powders and process-sampled particles associated with beryllium sensitization and CBD (Henneberger et al., 2001; Kreiss et al., 1997; Stange et al., 1996) were selected for study. The BeO powder was product type UOX-125 (Brush Wellman Inc., Elmore, OH), which is a high-purity end-product prepared (heat-treated) at 1150–1450 °C. The beryllium metal powder was product type I-400 (Brush Wellman Inc.), which is a high-purity end-product prepared from attritted metal chips. These powders represent the primary feed material for the manufacture of metal and oxide parts and are representative of powders used in the workplace. Samples of these powders were aerosolized at Lovelace Respiratory Research Institute (Albuquerque, NM) using a dry powder blower (Model 175, DeVilbiss, Somerset, PA) and aerodynamically size-separated using a five-stage aerosol cyclone (Smith et al., 1979) as previously described (Hoover et al., 1989; Stefaniak et al., 2004).

Process-sampled particles were emissions from a BeO powder production line and a copper–beryllium production line. Particles were sampled from a screener unit operation downstream of a calcine furnace (operating temperature 1150–1450 °C) in the BeO powder production line. Particles were also sampled from an arc furnace unit operation in a copper–beryllium alloy ingot production line. The operating temperature of the arc furnace is not precisely known but is estimated to exceed 2200 °C. Particles were collected with an aerosol cyclone from the ventilation ductwork of the screener unit operation in the BeO powder production line and the master alloy arc furnace unit operation in a copper–beryllium alloy ingot production line as previously described (Stefaniak et al., 2003, 2004).

Fig. 1 illustrates morphology of the materials determined using transmission electron microscopy (Model CM30 electron microscope, Philips Electron Optics,

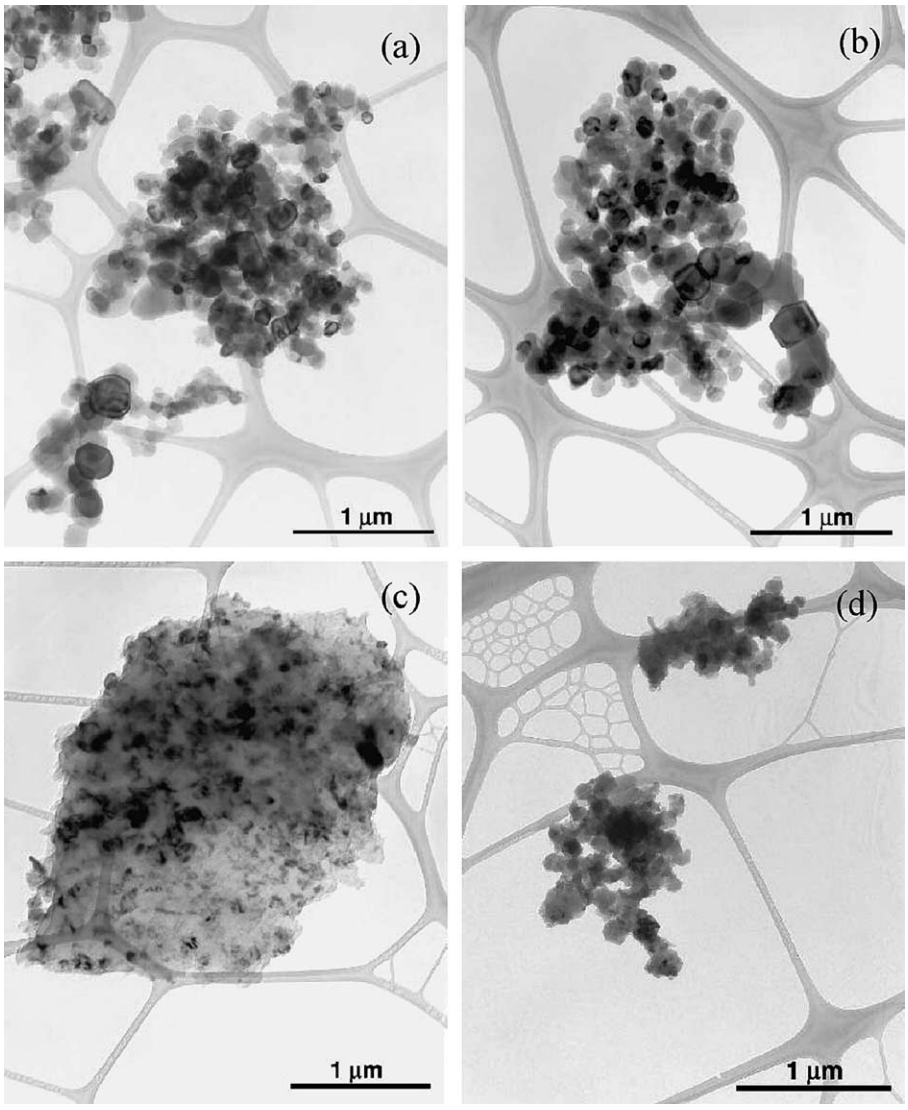

Fig. 1. Transmission electron microscope photomicrographs of (a) screener particles, (b) oxide powder, (c) metal powder, and (d) arc furnace particles. Beryllium aerosol materials had different morphology: screener particles, oxide powder, and arc furnace particles were agglomerate clusters of primary particles while metal powder was compact.

Eindhoven, The Netherlands). The BeO materials were clusters of primary particles, beryllium metal powder was compact, and arc furnace were also clusters of primary particles.

2.3. Dissolution solvent

Phagolysosomal simulant fluid (PSF) was used for this study because its pH matches that of phagolysosomes (pH 4.5) and because it has previously been evaluated in dissolution studies of beryllium aerosol materials (Stefaniak et al., 2005). The chemical composition of 0.02-M potassium hydrogen phthalate buffered PSF is presented as Table 1. Analytical grade chemicals (Fisher Scientific, Fairlawn, NJ) were used to prepare the PSF. As in previous dissolution studies, 50-ppm alkylbenzyldimethylammonium chloride (ABDC) was added as an antifungal agent (Finch et al., 1988). The

Table 1
Composition of 0.02-M potassium hydrogen phthalate buffered phagolysosomal simulant fluid

Constituent	mg/L
Sodium phosphate dibasic anhydrous (Na_2HPO_4)	142.0
Sodium chloride (NaCl)	6650.0
Sodium sulfate anhydrous (Na_2SO_4)	71.0
Calcium chloride dihydrate ($CaCl_2 \cdot 2H_2O$)	29.0
Glycine ($C_2H_5NO_2$)[a]	450.0
Potassium hydrogen phthalate (1-(HO_2C)-2-(CO_2K)-C_6H_4)	4084.6
Alkylbenzyldimethylammonium chloride (ABDC)[b]	50 ppm

[a] Representative of organic acids.
[b] Added as an antifungal agent.

initial pH of the PSF was typically 4.0. The solvent pH was raised to 4.5 by adding 0.1-M potassium hydroxide while monitoring using a calibrated pH electrode connected to a meter (Model AB15, Fisher Scientific) according to United States Environmental Protection Agency (US EPA) Method 9040B: pH electrometric measurement (US EPA, 1996).

2.4. Static dissolution technique

A static dissolution technique was chosen for the experiments because it is a well-established method for evaluating the dissolution behavior of relatively insoluble materials (Kanapilly et al., 1973; Ansoborlo et al., 1999). In addition, a recent study using this technique yielded dissolution results for beryllium that were in agreement with beryllium dissolution results obtained in vitro using a monocyte-macropahge cell line (Stefaniak et al., 2005). Static dissolution chambers were prepared by placing a known mass of beryllium material on a 37-mm diameter cellulose sample pad (stock number AP10, Millipore, Bedford, MA) and inserting the filter between two 0.025-μm pore size 47-mm diameter mixed cellulose ester filters (Millipore) to form a sandwich (Stefaniak et al., 2005). The outer few millimeters of each 47-mm diameter sandwich was securely clamped in the o-ring seal between the retaining rings of a static dissolution chamber (Intox Products, Moriarity, NM). Each sandwich was then placed in a separate beaker containing 80 mL of PSF. This arrangement allows for free contact and diffusion of the solvent through both the top and bottom surfaces of the filter sandwich. Each beaker was covered and maintained at 37 °C in a water bath (Model 286, Precision, Winchester, VA) and the pH in each beaker was monitored daily using a calibrated pH electrode to verify that pH remained at 4.5 ± 0.1. After 10 days, the dissolution chambers were removed from their beakers and the solvent was transferred to separate borosilicate glass sample jars (Qorpak, Bridgeville, PA). (Use of a single-time point permitted the examination of many replicate samples and multiple beryllium materials. See the section below on determination of chemical dissolution rate constants for the rationale for selecting 10 days as the dissolution period for this particular study.) Samples were stored frozen at −5 °C until analysis for beryllium content using inductively coupled plasma-mass spectrometry (ICP-MS).

2.5. Mercer dissolution theory

The dissolution behavior of materials evaluated in this study was assumed to conform to the theory of Mercer (1967). According to Mercer (1967) dissolution theory, the mass fraction remaining from a single homogeneous particle at a time, t, is:

$$\frac{m}{m_0} = \left[1 - \frac{\alpha_s k t}{3\alpha_v \rho D_0}\right]^3, \tag{1}$$

where

m	mass of particle remaining
m_0	initial particle mass
α_s	surface shape factor
α_v	volume shape factor
k	chemical dissolution rate constant, $\frac{\text{mass}}{\text{area}\cdot\text{time}}$
t	time
ρ	particle density
D_0	initial particle diameter

Mercer (1967) also describes an equation for the mass fraction remaining, $\frac{M}{M_0}$, from a log-normally distributed population of homogeneous particles characterized by a mass median diameter (D_m) and geometric standard deviation (σ_g):

$$\frac{M}{M_0} = \sum_{i=0}^{3} K_i \int_{y_i}^{\infty} f(y)\,dy, \tag{2}$$

where

$f(y)$	$\frac{1}{\sqrt{2\pi}}\exp\left(-\frac{y^2}{2}\right)$
K_0	1
K_1	$-\beta\exp(0.5\sigma^2)$
K_2	$\left(\frac{\beta^2}{3}\right)\exp(2\sigma^2)$
K_3	$-\left(\frac{\beta^3}{27}\right)\exp(4.5\sigma^2)$
σ	$\ln\sigma_g$
β	$\frac{\alpha_s k t}{\alpha_v \rho D_m}$
y_i	$\left(\frac{1}{\sigma}\right)\ln\left(\frac{\beta}{3}\right) + i\sigma$

Using Eq. (2), Mercer (1967) calculated $\frac{M}{M_0}$ as a function of β for σ ranging from 0.5 to 1.0 (i.e., σ_g ranging from 1 to 2.7). Mercer (1967) demonstrated that for values of β up to 6 and values of σ in the range 0.5–1.0, the integrals for $\frac{M}{M_0}$ in Eq. (2) could be approximated by the sum of two exponentials:

$$\frac{M}{M_0} = f_1\exp(-\lambda_1\beta) + f_2\exp(-\lambda_2\beta), \tag{3}$$

where the constants f and λ are determined by curve fitting for the value of σ_g under consideration.

According to Eq. (3), for $\sigma = 0.5$, $\frac{M}{M_0}$ is approximated by a single exponential, i.e., a straight line on a log-linear plot. For values of σ larger than 0.5, the second exponential term is needed to approximate the $\frac{M}{M_0}$ behavior for large β (Fig. 2). Note that the purpose of the second exponential term is to account for the shift in dissolution from small particles in the size distribution, which initially dominate dissolution, to large particles in the distribution, which dominate dissolution for larger values of β at later dissolution times. This shift in dissolution behavior is a manifestation of the kinetics,

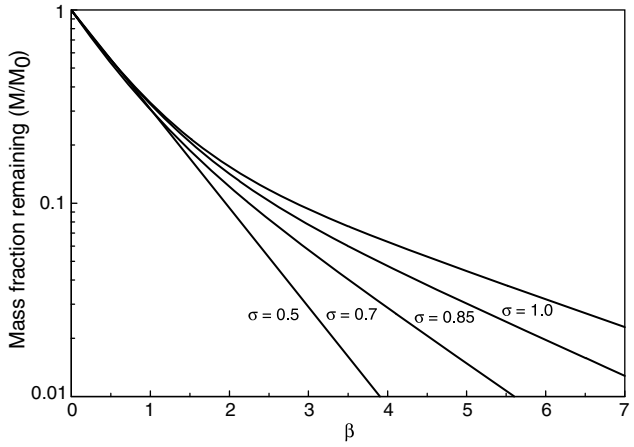

Fig. 2. Mass fraction remaining ($\frac{M}{M_0}$) for a log-normally distributed population of homogeneous particles as a function of β and σ according to Eq. (3) (adapted from Mercer, 1967).

which are dependent on the specific surface area (SSA) of the particle population and the surface area distribution of the particles. For a log-normal distribution, initial dissolution rate is dominated by the contributions from smaller particles, where the bulk of the surface area resides. As dissolution proceeds, the smallest particles are removed from the population through complete dissolution and the particle population distribution shape undergoes a transition, with the distribution mode shifting to the larger particles, which have high mass and low SSA. For $\sigma = 0.5$, the transition in particle population distribution shape takes place at values of $\frac{M}{M_0}$ less than 0.1 and at values of β larger than 1.5 (Fig. 2). As σ increases above 0.5, the log-normal size distribution skews toward the larger particles and the transition takes place at values of $\frac{M}{M_0}$ less than 0.3 and at values of β from 1.5 to 6. Thus, by limiting our data analysis to values of $\frac{M}{M_0}$ greater than 0.3, values of β less than 1.5, and a value of $\sigma = 0.5$ a single exponential term can be used to characterize our dissolution results. Using values of the constants f_1 and λ_1 provided by Mercer (1967) for $\sigma = 0.5$, Eq. (3) reduces to:

$$\frac{M}{M_0} = f_1 \exp(-\lambda_1 \beta) = 1.0 \exp(-1.18\beta). \tag{4}$$

According to Mercer (1967), if information regarding α_s and α_v is lacking for a material, the SSA of the material can be measured, and the following relationship for a log-normal distribution:

$$\frac{\alpha_s}{\alpha_v \rho D_m} = \mathrm{SSA} \exp\left(\frac{-\sigma^2}{2}\right), \tag{5}$$

where SSA = specific surface area, substituted into Eq. (4) to obtain:

$$\frac{M}{M_0} = \exp\left\{-1.18kt\,\mathrm{SSA} \exp\left(-\frac{\sigma^2}{2}\right)\right\}, \tag{6}$$

which reduces to

$$\frac{M}{M_0} = \exp(-1.04kt\,\mathrm{SSA}). \tag{7}$$

Thus, for the conditions studied, dissolution of a material depends on its chemical dissolution rate constant (k) value, a constant unique to a given chemical form of material and SSA.

To ensure compliance with the boundary condition of Eq. (7) for evaluating dissolution data (σ_g of 1–2.72), estimates of σ_g, along with the count median diameter (CMD), were made by measuring the Feret's diameter (Hinds, 1999) of $n = 1000$ particles of each study material. Particle sizing was performed using a filar ocular micrometer eyepiece (GEK, Inc., Charlottesville, VA) attached to a phase contrast microscope (Carl Zeiss, Inc., Germany).

Eq. (7) can also be expressed as the ratio of mass dissolved, M_D, to the initial mass M_0:

$$\frac{M_D}{M_0} = 1 - \exp(-1.04\,\mathrm{SSA}\,kt). \tag{8}$$

This equation provides a convenient method for calculating an estimate of the fraction of material dissolved in a period of time based on the SSA of the sample material and its value of k.

Eq. (7) can be rearranged to solve for k:

$$k = \frac{-\ln\left(\frac{M}{M_0}\right)}{1.04\,\mathrm{SSA}\,t}. \tag{9}$$

Similarly, Eq. (8) can be rearranged to solve for k if available data were in terms of the amount of material dissolved.

2.6. Determination of chemical dissolution rate constants (k)

Values of k were calculated for four different beryllium aerosol materials: screener particles, oxide powder, metal powder, and arc furnace particles (Table 2). The screener particles and oxide powder are single-constituent materials of BeO, the metal powder is a single-constituent material of beryllium metal, and the arc furnace particles are a multi-constituent material consisting of BeO and copper oxides (Stefaniak et al., 2004). The SSA for these materials were determined previously by nitrogen gas adsorption using the Brunauer, Emmett and Teller method. Triplicate surface area measurements were performed for each material using a calibrated surface area analyzer (Model MS-16, Quantachrome Corp., Syossett, NY). Estimates of surface area obtained were in agreement with values predicted from a theoretical geometric model (Stefaniak et al., 2003). Values of SSA for the study materials are provided in Table 2.

Table 2
Physicochemical properties of beryllium aerosol materials, initial beryllium mass, and calculated values of the chemical dissolution rate constant

Beryllium material[a]	Composition[b]	SSA (m^2/g)[c]	Size[d]		Initial mass		k [$g/(cm^2\ day)$][e]	
			CMD (μm)	σ_g	Particulate[f] (μg)	Beryllium[g] (μg)	Trial	Pooled
Screener particles	BeO	11.9 ± 0.0	1.1	1.6	168	59.5 ± 1.9	$1.0 \pm 0.7 \times 10^{-8}$	$1.3 \pm 1.9 \times 10^{-8}$
					504	163.4 ± 5.6	$1.1 \pm 0.4 \times 10^{-8}$	
					1008	261.8 ± 27.3	$1.9 \pm 3.2 \times 10^{-8}$	
Oxide powder	BeO	11.1 ± 0.0	1.2	1.5	180	56.3 ± 1.2	$1.2 \pm 0.5 \times 10^{-8}$	$1.1 \pm 0.5 \times 10^{-8}$
					539	184.6 ± 10.7	$1.1 \pm 0.3 \times 10^{-8}$	
					1077	300.4 ± 20.5	$0.9 \pm 0.4 \times 10^{-8}$	
Metal powder	Be	7.6 ± 0.1	3.0	1.8	385	368.0 ± 14.8	$1.0 \pm 1.1 \times 10^{-7}$	$1.1 \pm 1.4 \times 10^{-7}$
					1156	1043.3 ± 92.9	$1.5 \pm 2.0 \times 10^{-7}$	
					2313	2110.0[h]	$0.8 \pm 1.1 \times 10^{-7}$	
Arc furnace particles	Cu_2O, CuO, BeO	4.4 ± 0.0	1.9	1.7	450	20.9 ± 0.29	$2.1 \pm 0.8 \times 10^{-7}$	$1.6 \pm 0.6 \times 10^{-7}$
					1351	64.6 ± 3.55	$2.3 \pm 0.7 \times 10^{-7}$	
					2703	82.2 ± 13.9	$1.6 \pm 0.5 \times 10^{-7}$	

[a] Beryllium aerosol material was collected in stage-2 (metal powder) and stage-3 (screener oxide particles, oxide powder, and arc furnace particles) of aerosol cyclones as previously described (Hoover et al., 1989; Stefaniak et al., 2003, 2004).

[b] Compositions were determined using X-ray diffraction, transmission electron microscopy-selected area electron diffraction, and transmission electron microscopy-microelectron diffraction as first reported in Stefaniak et al. (2004). BeO = beryllium oxide, Be = beryllium, Cu_2O = copper(I) oxide, CuO = copper(II) oxide.

[c] Measured values of specific surface area (SSA) were first reported in Stefaniak et al. (2003).

[d] Count median diameter (CMD) and geometric standard deviation (σ_g) calculated from $n = 1000$ counts of Feret's diameter.

[e] Arithmetic mean ± standard deviation; within each beryllium material, values of k calculated at the low, medium, and high initial beryllium mass (M_0) trials were not statistically different and data were pooled to calculate an average value of k for each material.

[f] Initial particulate mass estimated from the volume of gravimetrically prepared suspension pipetted onto static dissolution chambers.

[g] Initial beryllium mass (M_0) measured using inductively coupled plasma-mass spectroscopy for $n = 5$ replicate static dissolution chambers of each material prepared at the time of experimental setup.

[h] Initial beryllium mass (M_0) measured using inductively coupled plasma-mass spectroscopy for $n = 1$ static dissolution chamber of this material prepared at the time of experimental setup for this dose level.

For each aerosol material, k was determined for 11 replicate static dissolution chambers at each of three initial mass levels, M_0 (Table 2). The value 11 was the result of a sample size calculation (Snedecor and Cochran, 1967) with probability of a type 1 error set to 0.05, probability of a type II error set to 0.05, and coefficient of variation of the ICP-MS analytical method set at 20%. The calculation also assumed an expected difference in dissolution of 30% between beryllium metal and BeO based on the data of Finch et al. (1988).

The data of Finch et al. (1988) also provided insight into the feasibility of obtaining the desired dissolution information using a short-term dissolution screening test, as well as insight into the appropriate time-point for the dissolution test. Finch et al. (1988) reported single-phase dissolution for beryllium metal, which means that any dissolution period long enough to obtain quantifiable dissolved beryllium could be used. Their results for high-fired BeO were biphasic, with the long-term (dominant) dissolution phase being well established within only a few days which means that a study duration of a week or more could be appropriate. Eq. (8) was used to calculate the amount of material expected to be dissolved as a function of time assuming the measured values of SSA for the beryllium metal, BeO, and arc furnace materials, and an upper limit k value of 10^{-9} $g/(cm^2\ day)$ determined by Finch et al. (1988) for BeO at neutral pH. In this manner, it was determined that a 10 day test duration was adequate to ensure that the amount of material dissolved from an initial mass of several milligrams during the study period would be greater than our detection limit for ICP-MS (see below). The exact values of M_0 for each sample material were then calculated using Eq. (7).

Each value of M_0 was quantified by analyzing five additional replicate filter sandwiches of each material prepared at the time of experimental setup. Using three particulate mass levels (nominally 1×, 3×, and 6× the lowest value of M_0) allowed evaluation of the dynamic range of the protocol (i.e., from dissolution levels near the detection limit to much greater than the detection limit) and of the assumption that the measured values of k will be independent of M_0 (i.e., in accordance with Mercer dissolution theory). Two field blank static dissolution chambers were included at each mass level. Eq. (9) was used to calculate values of k for each beryllium material at each M_0. The values of M for use in Eq. (9) were calculated using the relationship $M = M_0 - M_D$, where M_D was the mass of beryllium dissolved in PSF.

2.7. Further investigation of dissolution behavior for a multi-constituent material

The role of material and surface composition in beryllium dissolution was investigated using oxide powder (a single-constituent BeO material) and arc furnace particles (a multi-constituent material containing BeO) (Table 3). The hypothesis was that the dissolution behavior of the oxide powder can be accurately predicted based on knowledge of the material specific value of k and SSA but that the dissolution of beryllium from the arc furnace particles will be incorrectly estimated based on the k value for BeO and the measured SSA of the multi-constituent material.

High-resolution X-ray photoelectron spectroscopy (XPS) (Model PHI 5600, Perkin–Elmer Corp., Eden Prairie, MN, with a 1253.6-eV MgK-alpha X-ray source) was used to determine the chemical composition and relative percent abundance of elements on the outer 50–75 Å surface layers of oxide powder and arc furnace particles. Samples were prepared as thin layers of material on carbon tape adhered to a stainless steel shim. Charge-corrected spectra were compared to the published reference spectra of Moulder et al. (1992). XPS measurements were also made on samples of the beryllium metal powder and the thickness of the beryllium oxide surface layer was calculated using standard assumptions that the oxide layer was coherent (no breaks) and that the "take-off" angle for emitted electrons was 45°.

Dissolution was measured for 14 replicate samples of each study material at each of three particle sizes (Table 3). The sample size for this experiment was increased from 11 to 14 to ensure that in the event of a mishap (filter tear, etc.), although rare, a statistically valid data set would still be obtained. Inclusion of multiple particle sizes permitted determination of whether effective BeO SSA was strongly dependent on small changes in particle size. Although the CMDs of the BeO powder and the arc furnace particles were similar, the σ_g values were less than 2 and the 95% confidence intervals (Silverman et al., 1971) for the CMD values did not overlap. Each value of M_0 was quantified by analyzing five additional replicate filter sandwiches of each material prepared at the time of experimental setup. Two field blank static dissolution chambers were included at each particle size.

Eq. (8) was used to calculate the expected $\frac{M_D}{M_0}$ for each sample based on $t = 10$ days, the SSA of the sample material, and the mean value of k for the oxide powder from the previous experiment (Table 2). Eq. (8) was then rearranged to calculate the "effective" SSA (SSA_{eff}) that would correspond to the value of k for BeO (as determined in the previous experiment) and the measured values of $\frac{M_D}{M_0}$ from this experiment:

$$\text{Effective SSA} = \frac{-\ln\left(1-\frac{M_D}{M_0}\right)}{1.04kt}. \quad (10)$$

The expected values of $\frac{M_D}{M_0}$ at $t = 10$ days were then compared to the measured values of $\frac{M_D}{M_0}$, and the material

Table 3
Physicochemical properties of beryllium aerosol materials used to calculate beryllium oxide effective specific surface area

Beryllium material[a]	Composition[b]	SSA (m^2/g)[c]	Size[d]		Surface[e]		$\frac{M_D}{M_0}$[f]		Effective SSA (m^2/g)[g]
			CMD (μm)	σ_g	Composition	Be/Cu ratio	Expected	Measured	
Oxide powder	BeO	11.1 ± 0.0	1.4	1.5	–		0.013	0.012 ± 0.006	10
	BeO	11.1 ± 0.0	1.2	1.5	BeO		0.013	0.019 ± 0.009	15
	BeO	10.7 ± 0.0	1.0	1.4	–		0.012	0.018 ± 0.004	15
Arc furnace particles	–	3.7 ± 0.0	2.1	1.9	BeO, CuO	2.1	0.004	0.067 ± 0.044	56
	Cu_2O, CuO, BeO	4.4 ± 0.0	1.9	1.7	BeO, CuO	3.1	0.004	0.111 ± 0.038	94
	–	3.9 ± 0.0	1.6	1.7	BeO, CuO	2.3	0.005	0.153 ± 0.040	130

–: Not determined for this size of material.

[a] Beryllium aerosol material was collected in stage-2, 3, and 4 of aerosol cyclones as previously described (Hoover et al., 1989; Stefaniak et al., 2003, 2004).

[b] Compositions were determined using X-ray diffraction, transmission electron microscopy-selected area electron diffraction, and transmission electron microscopy-microelectron diffraction; BeO = beryllium oxide, Cu_2O = copper(I) oxide, CuO = copper(II) oxide. Ratio of total beryllium atoms to copper atoms in particle bulk ranged from 1.1 to 1.6, as determined using inductively coupled plasma-mass spectroscopy. Data were first reported in Stefaniak et al. (2004).

[c] Measured values of specific surface area (SSA) were first reported in Stefaniak et al. (2003).

[d] Count median diameter (CMD) and geometric standard deviation (σ_g) calculated from $n = 1000$ counts of Feret's diameter.

[e] Identity of atoms in the surfaces (outer 50–75 Å layer) and their chemical state determined using X-ray photoelectron spectroscopy. BeO = beryllium oxide, CuO = copper(II) oxide.

[f] Expected values of the mass fraction dissolved were calculated using Eq. (8) with the value of k for oxide powder determined in the initial experiment (Table 2), measured SSA for the material of interest and $t = 10$ days.

[g] Effective specific surface area (SSA) were calculated using Eq. (10) with the value of k for oxide powder determined in the initial experiment (Table 2) and measured values of the mass fraction dissolved for the material of interest.

specific values of SSA (Table 3) were compared to the calculated values of SSA_{eff} for the single-constituent and multi-constituent materials. Note that calculation of SSA_{eff} required the assumptions that all beryllium in arc furnace particles was in the form of BeO and that k for beryllium dissolution from arc furnace particles was the same as k for beryllium dissolution from oxide powder.

2.8. Beryllium analysis and quality control

All samples were submitted to Carlsbad Environmental Monitoring and Research Center (Carlsbad, NM) for analysis of beryllium content. Quality control samples included field blank samples, reagent blank samples (PSF or filters), and spike and split samples prepared gravimetrically using a beryllium standard reference material (SRM3105a, National Institute of Standards and Technology, Gaithersburg, MD). Liquid samples were analyzed by United States Environmental Protection Agency (US EPA) SW-846 Method 3015 (Microwave assisted acid digestion of aqueous samples and extracts). Filters were analyzed by US EPA SW-846 Method 3051 (Microwave assisted acid digestion of sediments, sludges, soils and oils) (US EPA, 1996). Both methods use a microwave digestion to completely dissolve beryllium oxide. The approach described in 40 CFR Part 136 was used to calculate the method detection limits of 1.56 μg beryllium/L and 0.006 μg beryllium/filter. These calculations involved taking the standard deviation from analysis of seven replicate aliquots of a beryllium standard prepared at five times the instrument limit of detection and multiplying it by 3.14, which is the Student's t-value for a sample size of seven (40 CFR 136.2).

Statistical comparisons were made using one-way analysis of variance (ANOVA) assuming that dissolution data were normally distributed and using the distribution-free Wilcoxon rank-sum test. For both statistical techniques, a significance level of $\alpha = 0.05$ was used for comparisons and Bonferroni corrected (Pagano and Gauvreau, 1992) as appropriate. Statistical analyses were performed using Stata (Version 7.0, StataCorp, College Station, TX). Note that results of statistical comparisons were independent of the assumed shape of the underlying distribution of the dissolution data, and for clarity, only results of the ANOVA analyses are reported.

3. Results

3.1. Compliance of material parameters with Mercer theory

The material property conditions required for use of Eq. (7) to evaluate dissolution data (σ_g of 1–2.72 and $\frac{M}{M_0} > 0.3$) were satisfied for the study materials. The σ_g ranged from 1.4 to 1.9 (see Tables 2 and 3) and $\frac{M}{M_0}$ calculated from the dissolution data ranged from 0.66 to 0.99.

3.2. Measured chemical dissolution rate constants

Values of k were normally distributed for each study material as shown by the plot in Fig. 3. Within each beryllium material, values of k calculated at the low, medium, and high M_0 were not statistically different, so data were pooled to calculate an average value of k for each material (Table 2). The values of k, in g/(cm^2 day), for BeO particles released from the screener unit operation ($1.3 \pm 1.9 \times 10^{-8}$) and for the finished product oxide powder ($1.1 \pm 0.5 \times 10^{-8}$) were similar ($p = 0.45$). Pooling data for the two oxides yielded an overall $k = 1.2 \pm 1.4 \times 10^{-8}$ g/(cm^2 day) for BeO. The value of k calculated for the finished product beryllium metal powder ($1.1 \pm 1.4 \times 10^{-7}$) was significantly greater than observed for the BeO materials ($p < 0.0003$). The value of k ($1.6 \pm 0.6 \times 10^{-7}$) for the arc furnace particles was significantly greater than observed for single-constituent BeO ($p < 0.00001$), despite the fact that the chemical form of beryllium in the aerosol was BeO.

3.3. Particle surface properties

Fig. 4 is high-resolution XPS spectra for the binding energy region of beryllium obtained from the surfaces (outer 50–75 Å layer) of oxide powder, beryllium metal powder, and arc furnace particles. The surface layer of

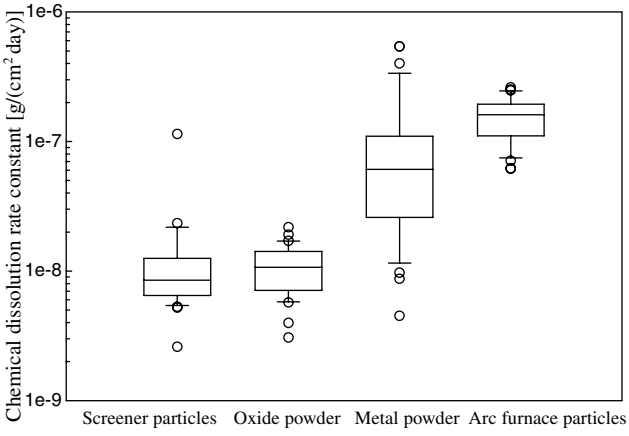

Fig. 3. Box plots of calculated k values for screener particles ($n = 33$), oxide powder ($n = 33$), metal powder ($n = 33$), and arc furnace particles ($n = 33$) in macrophage phagolsysosomal simulant fluid. The center of each box is the median, the top and bottom of each box are the 75th and 25th percentile, respectively; ends of the whiskers are 1.5 times the interquartile range; and values beyond the whiskers (''outliers'') are shown as open circles. The average value of k for the beryllium metal powder was significantly greater than observed for the beryllium oxide materials ($p < 0.0003$). The average value of k for the arc furnace particles was significantly greater than observed for the beryllium oxide materials ($p < 0.00001$).

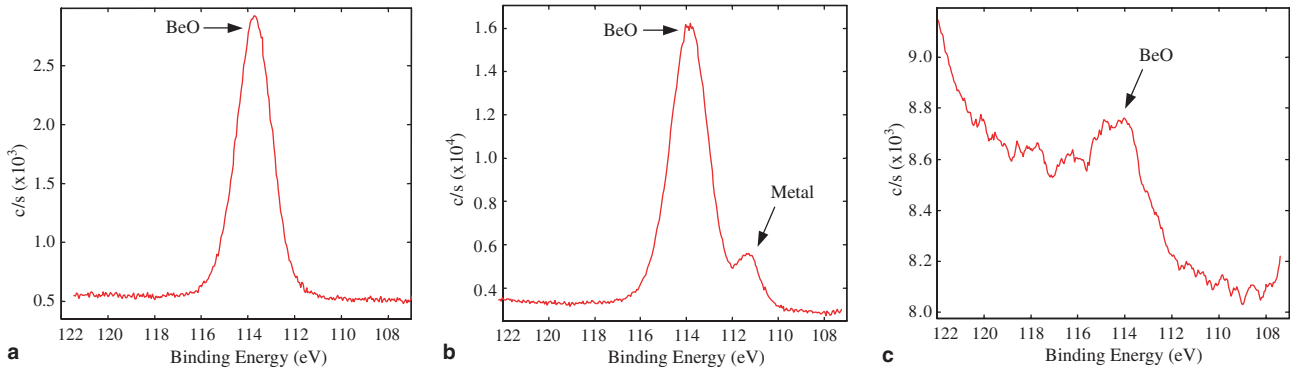

Fig. 4. High-resolution X-ray photoelectron spectra from the binding energy region of beryllium that were obtained from material surfaces (outer 50–75 Å layer) illustrating that (a) the surface of oxide powder was exclusively beryllium oxide, (b) the surface of metal powder was predominantly beryllium oxide with beryllium, and (c) the surface of arc furnace particles contained beryllium only in the form of beryllium oxide.

the oxide powder was exclusively BeO. The surface of the metal powder was a mixture of beryllium metal and BeO, with the BeO concentrated in an outer surface layer calculated to be approximately 42 Å thick. The surface layer of the arc furnace particles contained beryllium in the form of BeO and copper in the form of CuO (copper data not shown). The shapes of the high-resolution XPS spectra from the beryllium and copper binding energy regions were identical for the three sizes of arc furnace particles (data not shown), but differed in their peak intensities as indicated by the variation in the ratio of beryllium to copper atoms presented in Table 3; the spectra in Fig. 4 was from material with CMD = 1.8 μm.

3.4. Calculated effective BeO SSA

Table 3 contains the expected and measured beryllium mass fraction dissolved, $\frac{M_D}{M_0}$, from the three sizes of oxide powder and arc furnace particles, as well as the calculated SSA_{eff} for these study materials. Good agreement was observed between measured and predicted values of $\frac{M_D}{M_0}$ for all sizes of oxide powder studied; measured values of SSA were equal to SSA that governed beryllium dissolution, i.e., within 40% of calculated values of SSA_{eff}. In contrast, for all sizes of arc furnace particles studied, measured values of $\frac{M_D}{M_0}$ were one to two orders of magnitude higher than the predicted values.

4. Discussion

4.1. Compliance of material parameters with Mercer theory

Because the particles used in the current study were aerodynamically size-fractionated with an aerosol cyclone, the σ_g of the particle samples (1.4–1.9; see Tables 2 and 3) were smaller than the expected σ_g for the entire particle size distribution, and, therefore, easily complied with the material property conditions required for use of Eq. (7) to evaluate dissolution data (σ_g of 1–2.72 and $\frac{M}{M_0} > 0.3$). It is interesting to note that the material property condition requirement of Eq. (7) includes the σ_g value of 2.5, which the Human Respiratory Tract Model of the International Commission on Radiological Protection (ICRP, 1994) considers to be typical for workplace aerosols. The σ_g for beryllium aerosols measured in machining operations by Kelleher et al. (2001) were typically 2, with range 1.1–4.4.

4.2. Interpretation of chemical dissolution rate constant (k) values

For screener particles, oxide powder, and metal powder, the calculated values of k supported our assumption that material dissolution was in accordance with Mercer (1967) dissolution theory, i.e., k was independent of M_0 and measured values of SSA were equal to SSA that governed beryllium dissolution. For the arc furnace aerosol material, the calculated values of k did not support our assumption that material dissolution was in accordance with Mercer (1967) dissolution theory, i.e., although k for the mixture was independent of M_0, the measured values of SSA differed from the SSA that governed beryllium dissolution. As discussed below, we found that making a distinction between single- and multi-constituent materials was important for interpreting dissolution results for the arc furnace aerosol material.

4.2.1. Screener particles and oxide powder

The screener particles and oxide powder were single component materials (Stefaniak et al., 2004) with nearly identical measured SSA contributed by primary particle size (Stefaniak et al., 2003). There was no difference in k values between these materials (Table 2). Thus, in this

case it appears that the fugitive aerosol material is similar to the process material. As expected, the k value of $1.2 \pm 1.4 \times 10^{-8}$ g/(cm^2 day) for the BeO materials in PSF (pH 4.5) was greater than the historical value of $3.7 \pm 1.2 \times 10^{-9}$ reported by Finch et al. (1988) for BeO in a simulant of extracellular lung fluid (pH 7.3). Similarly, the value of k in PSF was less than the historical value of $6.1 \pm 2.2 \times 10^{-8}$ reported by Finch et al. (1988) for dissolution of BeO material in a more acidic, but less physiologically relevant, HCl solvent system (pH 1). Additionally, k determined in PSF was nearly identical to k determined for BeO in vivo using beagle dogs, $0.7 \pm 1.0 \times 10^{-8}$ (Finch et al., 1990), and was within a factor of two of the k determined for BeO in vitro using the J774A.1 murine monocyte-macrophage cell line, $2.3 \pm 1.9 \times 10^{-8}$ (Day et al., 2005).

4.2.2. Beryllium metal powder

Our results for the solubility of metal powder and BeO in PSF (pH 4.5) showed that beryllium metal dissolution was intrinsically greater than BeO dissolution. This finding is consistent with the Finch et al. (1988) studies that showed k values for metal powder were also greater than for BeO using serum ultrafiltrate (SUF) (pH 7.3), a simulant of extracellular lung fluid, and HCl (pH 1) solvents. Similar to the rank order of solubilities for BeO in the various solvents, the dissolution of metal powder was lowest in SUF, $k = 1.5 \pm 0.8 \times 10^{-9}$ g/(cm^2 day) (Finch et al., 1988), intermediate in PSF, $k = 1.1 \pm 1.4 \times 10^{-7}$ (this study), and highest in more acidic HCl, $k = 4.1 \pm 0.2 \times 10^{-7}$ (Finch et al., 1988).

Note that the presence of an oxide coating on the surface of metal powder did not result in the dissolution behavior of metal powder being identical to that of BeO. Despite the presence of a BeO layer approximately 40 Å thick, k determined for metal powder was an order of magnitude greater than k for BeO. Note also the excellent agreement between measured values of the oxide layer thickness in the current study using XPS (42 Å) and previous measurements (52 Å) using neutron activation analysis (Hoover et al., 1989). Using 52 Å as the upper bound estimate of the oxide layer thickness, the mass fraction of oxide on the surface of the metal powder under study was approximately 10% of the total particle mass (Hoover et al., 1989). After the 10 day study period, a spherical BeO particle having an initial diameter of 3.0 μm and the characteristic k value of the BeO materials ($k = 1.2 \times 10^{-8}$ g/(cm^2 day)) would have diameter 2.9992 μm (Eq. (1)), which is only 8 Å smaller than the initial diameter. Thus, if the oxide layer on metal powder had the same refractory characteristic as the BeO materials, then the PSF solvent would only have dissolved a fraction (4 Å/52 Å = 8%) of the estimated 52-Å thick layer of oxide on the surface. Based on the actual observed dissolution behavior of metal powder ($k = 1.1 \times 10^{-7}$ g/(cm^2 day)), a spherical metal particle having an initial diameter of 3.0 μm would have been dissolved to a diameter of 2.9890 μm (Eq. (1)), which is a calculated reduction in diameter of 110 Å. Note that this calculated reduction in diameter is only slightly greater than the reduction in diameter needed to remove the entire thickness of the unintentionally formed surface oxide layer (52 Å + 52 Å = 104 Å). These calculations support the conclusion that the quality of the unintentionally formed oxide layer on the surface of the metal powder is less durable than the oxide in the intentionally prepared BeO materials.

4.2.3. Arc furnace particles

The value of k determined using Mercer (1967) theory for dissolution of beryllium in the arc furnace aerosol material, $1.6 \pm 0.6 \times 10^{-7}$ g/(cm^2 day), was an order of magnitude greater than the value of k determined for the single-constituent BeO aerosol materials, $1.2 \pm 1.4 \times 10^{-8}$. This was despite the fact that BeO was the only chemical form of beryllium identified in arc furnace aerosol material. Therefore, as discussed below, the follow-on experiment was performed in which detailed information about the material and surface composition of the study materials were used to account for observed dissolution of the multi-constituent arc furnace particles.

4.3. Dissolution behavior of the multi-constituent material

The calculated values of k for the arc furnace aerosol material did not support our assumption that material dissolution was in accordance with Mercer (1967) dissolution theory. Although k for the mixture was independent of M_0, the measured values of SSA differed from the SSA that governed beryllium dissolution. One possible explanation for this deviation from Mercer (1967) dissolution theory may be due to an intrinsically greater solubility of the copper matrix of the arc furnace particles compared to the intrinsic solubility of the minor beryllium component. The fact that X-ray diffraction peaks consistent with BeO were generated from arc furnace particles indicated that BeO was at least several crystalline planes thick, and not as individual molecules dispersed throughout the particles. The observed segregation of BeO from copper oxides on the particle surface further supports the premise that BeO was present in the form of inclusions. Therefore, we hypothesize that the greater than expected solubility of beryllium from the arc furnace particles was the result of rapid dissolution of copper from the particles, which exposed small inclusions of BeO. These BeO inclusions would have higher SSA than measured for the total particle sample and would therefore dissolve at a proportionally higher rate. To test the hypothesis regarding the intrinsically

greater solubility of the copper matrix of the arc furnace particles, additional experimentation is needed to measure the simultaneous dissolution kinetics of copper and beryllium from arc furnace particles.

Note that the mechanism for enhanced dissolution of a metal in the presence of copper has been proposed by Brown et al. (1982) to explain the observation that more gold dissolves from higher-copper-content gold–copper alloys than from lower-copper-content gold–copper alloys in a 0.1 M glycine solvent. Hirano et al. (1993) observed that respirable, single-constituent CuO particles intratracheally instilled in rats cleared the lung with a half-time of 37 h. Benson et al. (2000) observed that 90% of copper in respirable particles of copper-beryllium alloy (nominal 98% copper, 2% beryllium) intratracheally instilled in rats cleared the lung with a half-time of 12–48 h, whereas the beryllium content of the particles cleared more slowly (half-time of several weeks).

4.4. Methodological issues

In the present study, k was estimated at a single-time point, i.e., day 10. This approach allowed for examination of many replicate samples and multiple beryllium materials. In general, dissolution is measured over a number of time points. Both single-phase and biphasic dissolution behavior have been observed for beryllium from single-constituent beryllium aerosol materials (Finch et al., 1988). In the case of single-phase dissolution, k is estimated using all of the dissolution data, whereas, if dissolution is biphasic, k is estimated from the data associated with the slower long-term dissolution phase. In the case of single-phase dissolution, collecting samples at a single time point, e.g., day 1 or day 10, should yield an unbiased estimate of k. For biphasic dissolution, measuring dissolution at a single-time point after the initial rapid phase may overestimate k for the slower long-term phase. However, in the current study, the single-time point approach resulted in estimates of k that were in agreement with existing beryllium dissolution data from the multi-time point studies of Finch et al. (1988, 1990). To estimate k in the present study, beryllium particles were sandwiched between two filters and the beryllium that dissolved from the particles and escaped to the free volume of the dissolution solvent was measured. A fundamental limitation of any dissolution technique that uses filters to prevent undissolved particulate material from entering the free volume of the dissolution solvent is the potential for dissolved material to adsorb to the filters. If material that dissolved from particles adsorbed to the filter sandwich, rather than escape to the free volume of the dissolution solvent, it would result in an underestimation of k by the dissolution technique. At low dissolution levels, the impact of dissolved material that adsorbs to the filter sandwich on k will be more pronounced than at high dissolution levels. However, in the current study, the estimates of k did not differ significantly as a function of initial mass within each beryllium study material (Table 2).

Regarding the calculation of SSA_{eff} for our assumed BeO inclusions in the arc furnace particles, there were two underlying assumptions. The first was that the chemical form of beryllium in both the oxide powder and in the arc furnace particles was the same, namely BeO. This condition was satisfied because the X-ray and electron diffraction analyses and the high-resolution XPS analyses demonstrated that BeO was the only form of beryllium in oxide powder and arc furnace particles. The second assumption was that k for beryllium dissolution from BeO in arc furnace particles was the same as k for beryllium dissolution from oxide powder. According to Mercer (1967) k will remain a constant as long as particle size is sufficiently large, i.e., greater than 10 nm. Based on the values of 56, 94, and 130 m^2/g for the SSA_{eff} of BeO in the arc furnace particles (Table 3), the calculated diameter of the inclusions based on a spherical model was 36, 21, and 15 nm, respectively. Therefore, the Mercer (1967) minimum-size condition was met. Note also that after the 10 day study period, a spherical BeO inclusion having an initial diameter of 15 nm and $k = 1.2 \times 10^{-8}$ g/(cm^2 day) would have diameter 14.2 nm (Eq. (1)), which is still larger than the 10 nm minimum.

Regarding the use of filters with a nominal pore size of 25 nm in the in vitro dissolution chambers, the possibility exists that some material may escape the dissolution chamber as molecular aggregates rather than as dissolved material. That is a fundamental limitation of any dissolution technique that uses filters to prevent undissolved material from entering the free volume of the dissolution solvent. However, the initial particle size was greater than 1 μm for the metal powder, greater than 200 nm for the BeO primary particles, and on the order of hundreds of nanometers for the arc furnace particles (see Fig. 1 and Table 2). In addition, after the 10 day study period, a spherical metal particle having an initial diameter of 1 μm and $k = 1.1 \times 10^{-7}$ g/(cm^2 day) would have diameter 0.99 μm and a spherical BeO primary particle having an initial diameter of 200 nm and $k = 1.2 \times 10^{-8}$ g/(cm^2 day) would have diameter 199 nm (Eq. (1)). Thus, concerns for overestimation of particle dissolution due to loss of sub-25-nm material from the dissolution chamber would only be associated with evaluation of the smallest postulated BeO inclusions of arc furnace particles. If such errors occurred, they would result in the overestimation of SSA_{eff}. It would be useful to assess changes in the particle size distribution of the arc furnace material over time. If a liquid particle spectrometer was capable of discriminating BeO inclusions from other chemical forms of colloids in the free volume of the solvent, it might

be possible to determine the size distribution of the BeO inclusions.

Regarding the observed independence of dissolution results as a function of initial beryllium mass in the dissolution chambers, values of k did not differ significantly as a function of initial mass within each study material (Table 2). This independence was despite the fact that the range of beryllium M_0 values used to determine k spanned an order of magnitude for metal powder and the beryllium oxide materials and a factor of four for arc furnace particles. These results provide guidance for appropriate selection of values of beryllium M_0 for design of future beryllium dissolution studies. For example, if the study material is plentiful, milligram amounts of material could be used in each dissolution chamber and acceptable analytical results might be possible with moderately sensitive analytical techniques. Conversely, if only small amounts of the study material are available, then equally reliable results might be obtained using tens of micrograms of initial mass in conjunction with more sensitive analytical techniques.

4.5. Implications for beryllium sensitization and CBD

The relevance of copper–beryllium aerosol solubility to health effects in exposed individuals needs to be explored. The question of whether the unexpected dissolution results for arc furnace particles were due to a multi-constituent aerosol in general, or to the copper–beryllium elemental content in particular, or to the furnace process that generated arc furnace particles, might be answered by collecting and characterizing samples of copper–beryllium aerosol from additional processes associated with prevalence of sensitization and CBD. Schuler et al. (2005) studied beryllium sensitization and CBD in a facility where semi-finished copper–beryllium is rolled into strip or drawn into wire. Although, the Schuler et al. (2005) work provides an epidemiologic basis for future sample collection, there are some significant methodological challenges to obtaining quantifiable aerosol samples. Airborne beryllium levels in the facility are very low (approximately 0.02 $\mu g/m^3$ of air), which will make collection of adequate mass quantities of material for physicochemical characterization and dissolution studies difficult. Note that the physicochemical characterization and dissolution studies described herein for the arc furnace particles required approximately 250 mg of material. Complex and expensive sampling strategies, e.g., use of an aerosol cyclone to collect particles from a more concentrated source than ambient workplace air such as the ventilation ductwork of an operation (Stefaniak et al., 2003, 2004), will be needed to obtain the necessary quantities of material for future studies.

Beryllium particles can be detected in the human lung several years after exposure has ceased (Dutra, 1948; Stoeckle et al., 1969; Williams and Wallach, 1989; Butnor et al., 2003). Data presented in this study for beryllium metal powder and for BeO suggest that beryllium particles retained in the lung may undergo dissolution slowly and could contribute to beryllium dosimetry for years after exposure has ceased. This hypothesized contribution of beryllium dissolution to lung dose is consistent with the findings of Fontenot et al. (1998) who observed that beryllium-specific CD4+ T-cells express a consistent repertoire of T-cell receptors in the lungs of persons with CBD for several years, which suggests a persistent specific provocation of the beryllium immune response.

5. Summary remarks

Dissolution rates were measured for single-constituent and multi-constituent beryllium aerosol materials using a simulant of phagolysosomal fluid with pH that is physiologically relevant and has not been previously used in beryllium dissolution studies. Results were modeled using a surface-area-proportional dissolution model. Beryllium materials known to be associated with beryllium sensitization and CBD have a range of physicochemical properties, which translate into different dissolution behaviors and different degrees of bioavailability. Consistent with previously published observations of the relative solubility of beryllium metal and beryllium oxide in a variety of solvents, values of the dissolution constant k for single-constituent beryllium metal in the simulated phagolysosomal fluid were significantly greater than for BeO. As expected, dissolution of both materials was greater in the simulated phagolysosomal fluid than previously published values in the more pH-neutral fluid of the extracellular lung environment, and less than dissolution in a more acidic HCl solvent. In addition, values of k were independent of the initial mass of material in the dissolution chamber, demonstrating the flexibility of requirements for initial mass and analytical sensitivity in the in vitro dissolution technique.

The rate of beryllium dissolution from the multi-constituent arc furnace particles was greater than expected compared to dissolution of the single-constituent beryllium oxide powder, despite the fact that the chemical form of beryllium in the arc furnace particles was beryllium oxide. This greater-than-expected beryllium solubility appears to stem from the bulk and surface composition of the study materials: it is likely that copper rapidly dissolves from the particles, thereby exposing the small inclusions of BeO which have higher SSA than measured for the total particle sample and therefore dissolve at a proportionally higher rate.

Additional studies of the dissolution behavior of beryllium materials in a variety of mixture configurations

(uniform mixtures, non-homogeneous mixtures, surface coatings, etc.) are needed to aid in developing exposure–response models to improve understanding of the risk of beryllium sensitization and CBD. Improved exposure–response models could provide a basis for understanding and managing process- or job-related risks for beryllium sensitization and CBD by using detailed information about the physicochemical form and bioavailability of the exposure material.

Acknowledgments

The authors thank B. Gallimore, R. Grundemann, and B. Hargis at LANL for their support and encouragement and Lovelace Respiratory Research Institute for assistance with the beryllium metal and oxide powders used in this study. We also thank R. Dickerson, E. Peterson, and R. Schulze at LANL for the microanalyses; J. Antonini, A. Miller, and J. Burkhart at NIOSH for their critical reviews of this manuscript, and C. Schuler and K. Kreiss at NIOSH for their support and useful discussion of this work. This project was supported primarily by NIOSH Research Grant 1R03 OH007447-01, and, by the LANL HSR Division TDEA program. A.B. Stefaniak also received support from NIEHS Training Program in Environmental Health Sciences ES07141.

References

Ansoborlo, E., Henge-Napoli, M.H., Chazel, V., Gibert, R., Guilmette, R.A., 1999. Review and critical analysis of available in vitro dissolution tests. Health Physics 77, 638–645.

Benson, J.M., Holmes, A.M., Barr, E.B., Nikula, K.J., March, T.H., 2000. Particle clearance and histopathology in lungs of C3H/HeJ mice administered beryllium/copper alloy by intratracheal instillation. Inhalation Toxicology 12, 733–749.

Brown, D.H., Smith, W.E., Fox, P., Sturrock, R.D., 1982. The reaction of gold (0) with amino acids and the significance of these reactions in the biochemistry of gold. Inorganica Chimica Acta 67, 27–30.

Butnor, K.J., Sporn, T.A., Ingram, P., Gunasegaram, S., Pinto, J.F., Roggli, V.L., 2003. Beryllium detection in human lung tissue using electron probe X-ray microanalysis. Modern Pathology 16, 1171–1177.

CFR, 1984. Code of Federal Regulations. Title 40, part 136.2, Guidelines establishing test procedures for the analysis of pollutants, Appendix B. US Government Printing Office, Washington, DC.

Day, G.A., Hoover, M.D., Stefaniak, A.B., Dickerson, R.M., Peterson, E.J., Esmen, N.A., Scripsick, R.C., 2005. Bioavailability of beryllium oxide particles: an in vitro study in the murine J774A.1 macrophage cell line model. Experimental Lung Research 31, 341–360.

Dutra, F.R., 1948. The pneumonitis and granulomatosis peculiar to beryllium workers. American Journal of Pathology 24, 1137–1165.

Eisenbud, M., 1998. The standard for control of chronic beryllium disease. Applied Occupational and Environmental Hygiene 13, 25–31.

Eidson, A.F., Taya, A., Finch, G.L., Hoover, M.D., Cook, C., 1991. Dosimetry of beryllium in cultured canine pulmonary alveolar macrophages. Journal of Toxicology and Environmental Health 34, 433–448.

Finch, G.L., Mewhinney, J.A., Eidson, A.F., Hoover, M.D., Rothenberg, S.J., 1988. In vitro dissolution characteristics of beryllium oxide and beryllium metal aerosols. Journal of Aerosol Science 19, 333–342.

Finch, G.L., Mewhinney, J.A., Hoover, M.D., Eidson, A.F., Haley, P.J., Bice, D.E., 1990. Clearance, translocation, and excretion of beryllium following acute inhalation of beryllium oxide by beagle dogs. Fundamental and Applied Toxicology 15, 231–241.

Fontenot, A.P., Kotzin, B.L., Comment, C.E., Newman, L.S., 1998. Expansions of T-cell subsets expressing particular T-cell receptor variable regions in chronic beryllium disease. American Journal of Respiratory and Cell and Molecular Biology 18, 581–589.

Henneberger, P.K., Cumro, D., Deubner, D.D., Kent, M.S., McCawley, M., Kreiss, K., 2001. Beryllium sensitization and disease among long-term and short-term workers in a beryllium ceramics plant. International Archives of Occupational and Environmental Health 74, 167–176.

Hinds, W.C., 1999. Aerosol Technology: Properties, Behavior, and Measurement of Airborne Particles, second ed. John Wiley & Sons, New York.

Hirano, S., Ebihara, H., Sakai, S., Kodama, N., Suzuki, K.T., 1993. Pulmonary clearance and toxicity of intratracheally instilled cupric oxide in rats. Archives of Toxicology 67, 312–317.

Hoover, M.D., Castorina, B.T., Finch, G.L., Rothenberg, S.J., 1989. Determination of the oxide layer thickness on beryllium metal particles. American Industrial Hygiene Association Journal 50, 550–553.

International Commission on Radiological Protection, 1994. Human Respiratory Tract Model for Radiological Protection. ICRP Publication 66, Elsevier Science, Tarrytown, NY, p. 49.

Kanapilly, G.M., Raabe, O.G., Goh, C.H., Chimenti, R.A., 1973. Measurement of in vitro dissolution of aerosol particles for comparison to in vivo dissolution in the lower respiratory tract after inhalation. Health Physics 24, 497–507.

Kelleher, P.C., Martyny, J.W., Mroz, M.M., Maier, L.A., Ruttenber, A.J., Young, D.A., Newman, L.S., 2001. Beryllium particulate exposure and disease relations in a beryllium machining plant. Journal of Occupational and Environmental Medicine. 43, 238–249.

Kreiss, K., Mroz, M., Zhen, B., Wiedemann, H., Barna, B., 1997. Risks of beryllium disease related to work processes at a metal, alloy, and oxide production plant. Occupational and Environmental Medicine 54, 605–612.

Maier, L.A., Newman, L.S., 1998. Beryllium disease. In: Rom, W.N. (Ed.), Environmental and Occupational Medicine Lippincott-Raven, Philadelphia, PA, pp. 1017–1031.

Mercer, T.T., 1967. On the role of particle size in the dissolution of lung burdens. Health Physics 13, 1211–1221.

Moulder, J.F., Stickle, W.F., Sobol, P.E., Bomben, K.D., 1992. In: Chastain, J. (Ed.), Handbook of X-ray Photoelectron Spectroscopy. Perkin Elmer Corp. Physical Electronics Division, Eden Prairie, MN.

Nyberg, K., Johansson, A., Camner, P., 1989a. Intraphagososmal pH in alveolar macrophages studied with fluorescein-labeled amorphous silica particles. Experimental Lung Research 15, 49–62.

Nyberg, K., Johansson, U., Rundquist, I., Camner, P., 1989b. Estimation of pH in individual alveolar macrophage phagolysosomes. Experimental Lung Research 15, 499–510.

Pagano, M., Gauvreau, K., 1992. Principles of Biostatistics. Duxbury Press, Belmont, CA, pp. 273–283.

Richeldi, L., Sorrention, R., Saltini, C., 1993. HLA-DPB1 Glutamate 69: a genetic marker of beryllium disease. Science 262, 242–244.

Schuler, C.R., Kent, M.S., Deubner, D.C., Berakis, M.T., McCawley, M., Henneberger, P.K., Rossman, M.D., Kreiss, K., 2005. Process-related risk of beryllium sensitization and disease in a copper–beryllium alloy facility. American Journal of Industrial Medicine 47, 195–205.

Silverman, L., Billings, C.E., First, M.W., 1971. Particle Size Analysis in Industrial Hygiene. Academic Press, New York, NY, pp. 251–253.

Smith, W.B., Wilson, R.R., Harris, D.B., 1979. A five-stage cyclone system for in situ sampling. Environmental Science and Technology 13, 1387–1392.

Snedecor, G.W., Cochran, W.G., 1967. Statistical Methods, sixth ed. Iowa State University Press, Ames, IA, p. 113.

Stange, A.W., Hilmas, D.E., Furman, F.J., 1996. Possible health risk from low-level exposure to beryllium. Toxicology 111, 213–224.

Stefaniak, A.B., Hoover, M.D., Dickerson, R.M., Peterson, E.J., Day, G.A., Breysse, P.N., Kent, M.S., Scripsick, R.C., 2003. Surface area of respirable beryllium metal, oxide, and copper alloy aerosols and implications for assessment of exposure risk of chronic beryllium disease. American Industrial Hygiene Association Journal 64, 297–305.

Stefaniak, A.B., Hoover, M.D., Day, G.A., Dickerson, R.M., Peterson, E.J., Kent, M.S., Schuler, C.R., Breysse, P.N., Scripsick, R.C., 2004. Characterization of physicochemical properties of beryllium aerosols associated with chronic beryllium disease. Journal of Environmental Monitoring 6, 523–532.

Stefaniak, A.B., Guilmette, R.A., Day, G.A., Hoover, M.D., Breysse, P.N., Scripsick, R.C., 2005. Characterization of simulated phagolysosomal fluid for study of beryllium dissolution. Toxicology in Vitro 19, 123–134.

Sterner, J.H., Eisenbud, M., 1951. Epidemiology of beryllium intoxication. A.M.A. Archives of Industrial Hygiene and Occupational Medicine 4, 123–151.

Stoeckle, J.D., Hardy, H.L., Weber, A.L., 1969. Chronic beryllium disease: long-term follow-up of sixty cases and selective review of the literature. American Journal of Medicine 46, 545–559.

United States Environmental Protection Agency, 1996. SW-846: Test Methods for Evaluating Solid Waste, Physical/Chemical Methods. US EPA Office of Solid Waste. Update III. National Technology Information Service, Springfield, VA.

Williams, W.J., Wallach, E.R., 1989. Laser microprobe mass spectrometry (LAMMS) analysis of beryllium, sarcoidosis, and other granulomatous diseases. Sarcoidosis 6, 111–117.